Article

Ab Initio Simulations of Poorly and Well Equilibrated $(CH_3CN)_n^-$ Cluster Anions: Assigning Experimental Photoelectron Peaks to Surface-Bound Electrons and Solvated Monomer and Dimer Anions

Published as part of The Journal of Physical Chemistry virtual special issue "Daniel Neumark Festschrift".

Wilberth A. Narvaez and Benjamin J. Schwartz*

Cite This: *J. Phys. Chem. A* 2021, 125, 7685−7693

Read Online

ACCESS | Metrics & More | Article Recommendations | SI Supporting Information

ABSTRACT: Excess electrons in liquid acetonitrile are of particular interest because they exist in two different forms in equilibrium: they can be present as traditional solvated electrons in a cavity, and they can form some type of solvated molecular anion. Studies of small acetonitrile cluster anions in the gas phase show two isomers with distinct vertical detachment energies, and it is tempting to presume that the two gas-phase cluster anion isomers are precursors of the two excess electron species present in bulk solution. In this paper, we perform DFT-based *ab initio* molecular dynamics simulations of acetonitrile cluster anions to understand the electronic species that are present and why they have different binding energies. Using a long-range-corrected density functional that was optimally tuned to describe acetonitrile cluster anion structures, we have theoretically explored the chemistry of $(CH_3CN)_n^-$ cluster anions with sizes n = 5, 7, and 10. Because

the temperature of the experimental cluster anions is not known, we performed two sets of simulations that investigated how the way in which the cluster anions are prepared affects the excess electron binding motif: one set of simulations simply attached excess electrons to neutral $(CH_3CN)_n$ clusters, providing little opportunity for the clusters to relax in the presence of the excess electron, while the other set allowed the cluster anions to thermally equilibrate near room temperature. We find that both sets of simulations show three distinct electron binding motifs: electrons can attach to the surface of the cluster (dipole-bound) or be present either as solvated monomer anions, CH_3CN^-, or as solvated molecular dimer anions, $(CH_3CN)_2^-$. All three species have higher binding energies at larger cluster sizes. Thermal equilibration strongly favors the formation of the valence-bound molecular anions relative to surface-bound excess electrons, and the dimer anion becomes more stable than the monomer anion and surface-bound species as the cluster size increases. The calculated photoelectron spectra from our simulations in which there was poor thermal equilibration are in good agreement with experiment, suggesting assignment of the two experimental cluster anion isomers as the surface-bound electron and the solvated molecular dimer anion. The simulations also suggest that the shoulder seen experimentally on the low-energy isomer's detachment peak is not part of a vibronic progression but instead results from molecular monomer anions. Nowhere in the size range that we explore do we see evidence for a nonvalence, cavity-bound interior-solvated electron, indicating that this species is likely only accessible at larger sizes with good thermal equilibration.
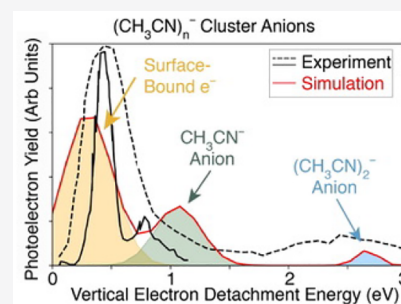
■ INTRODUCTION

Solvated electrons have been of great interest recently because they provide a paradigm system for confronting the predictions of quantum simulations with experiment. Typically when excess electrons are injected into a neutral liquid, they localize in a cavity in the liquid due to Pauli repulsive interactions from the surrounding closed-shell solvent molecules. However, in liquid acetonitrile (CH_3CN), an excess electron can also bind to one or more solvent molecules to create a solvated molecular anion. In fact, excess electrons in liquid acetonitrile take on two distinct forms that are in equilibrium with each other: a traditional solvated electron in a cavity in the liquid, which absorbs strongly in the near-infrared region,[1] and a solvated molecular anion, which absorbs weakly in the visible region.[2−4] At room temperature, the equilibrium constant

favors the solvated molecular anion species by a factor of roughly 4.[1,4] The precise identity of the molecular anionic species is still unknown, but it has been speculated that this species is likely a solvated molecular dimer anion, which would consist of two bent acetonitrile molecules oriented in an antiparallel manner.[5−7]

Because of the unique dual nature of excess electrons in liquid acetonitrile, there also has been recent interest in

acetonitrile cluster anions, $(CH_3CN)_n^-$, which should serve as precursors to the fully solvated species in the bulk liquid. Photoelectron spectroscopy experiments on acetonitrile cluster anions with sizes $n = 10-100$ revealed two peaks whose vertical electron detachment energies (VEDEs) differed by over 2 eV.[8] The lower-energy band, which is found between 0.4 and 1.0 eV depending on cluster size, is commonly labeled "isomer I", while the higher-energy peak, whose maximum is found between 2.5 and 3.0 eV, is termed "isomer II". For both isomers, the VEDE shifts to higher energies with increasing cluster size.[8] The same experiments found that smaller clusters ($n \leq 12$) favored the formation of isomer I, while the isomer II band dominated the photoelectron spectrum for sizes $n > 13$.[8] Furthermore, an additional weak peak was observed near ~0.8 eV for smaller cluster sizes, which has been assigned as a C−H vibronic excitation of isomer I.[8] Neumark and co-workers also applied time-resolved photoelectron imaging to acetonitrile cluster anions of sizes $n = 20-50$ to examine the excited-state dynamics of isomer II. These researchers found a lack of size dependence for the excited-state lifetime, suggesting a localized binding motif for this isomer.[9]

Of course, it is tempting to assign the two isomers seen in gas-phase $(CH_3CN)_n^-$ cluster anions as precursors of the two distinct excess electron species observed in the bulk liquid. This type of extrapolation also has been attempted for water cluster anions, which similarly show multiple isomers in photoelectron spectroscopy,[10−17] even though only a single type of hydrated electron is observed in aqueous solution.[18−21] However, theoretical calculations suggest that at small cluster sizes ($n \leq 20$) all of the different water anion cluster isomers have the excess electron residing on the surface of the cluster, so that the cluster behavior is not representative of interior states that would be present in bulk liquid water.[22] Moreover, calculations have shown that the different surface-bound isomers are created with different relative populations that depend on how the cluster anions were prepared; that is, the structural isomers observed depend on the temperature of the clusters,[22−24] which is generally not easily controllable or even known experimentally.

One previous theoretical attempt to understand the nature of excess electrons in acetonitrile cluster anions consisted of a mixed quantum-classical molecular dynamics simulation on clusters with sizes between $n = 5$ and 100.[25] These simulations employed a classical model for the acetonitrile molecules and a fixed pseudopotential for the classical acetonitriles' interaction with the quantum excess electron.[26,27] At larger cluster sizes, an internal cavity-solvated electron was observed, while metastable surface-bound states were seen for the smallest cluster sizes at low temperatures.[25] However, because an acetonitrile molecule's electron affinity increases as the molecule bends, such simulations are not capable of describing a solvated molecular anion. This is because the molecules that comprise the anion have a different electronic structure when they bend, allowing a partial C−C bond to be created between molecules, but this change in electronic structure cannot be described by using a pseudopotential optimized for the closed-shell, unbent molecule. Thus, the best that can be concluded from this study is that at larger sizes at room temperature a traditional cavity excess electron is a reasonable assignment for one of the two species observed in the bulk liquid.

Clearly, dynamical quantum chemistry studies on acetonitrile cluster anions would be of great help in identifying isomers I and II and their connection with the species in bulk

solution. To date, however, the calculations that have been performed were limited to static energetic studies on gas-phase molecular anions and clusters of small size ($n \leq 10$).[7,28−32] One set of cluster calculations at the MP2 and CCSD(T) level of theory identified a wide variety of dipole-bound anions for clusters with size $n = 2$ and 3.[28] Another set of calculations using the B3LYP and PW91 functionals showed that the dimer anion can become stable for clusters of size $n = 4-6$ if the surrounding solvent molecules interacted with the dimer's N atoms through an N···H interaction.[29] These same workers also demonstrated that if the geometry were appropriately constrained, an interior (i.e., "cavity-like") excess electron could be obtained for $(CH_3CN)_6^-$,[29] but it is unclear if such a binding motif is artificial or likely to be observed experimentally as it was not replicated for any other cluster size.

The aim of the present paper is to provide a firm theoretical assignment of the peaks observed in the $(CH_3CN)_n^-$ cluster anion photoelectron spectroscopy experiments through *ab initio* calculations. Cluster anions of sizes $n = 5, 7$, and 10 were simulated by using a long-range-corrected (LRC) DFT functional optimally tuned for this chemical system. Because the way in which cluster anions are produced affects their temperature and thus their electron binding motif(s), we have simulated the production of $(CH_3CN)_n^-$ structures with two different thermalization conditions. First, we ran Born−Oppenheimer molecular dynamics (BOMD) simulations of acetonitrile cluster anions at room temperature to study the limit of maximum possible equilibration and the best possible correspondence with the excess electron species in the bulk liquid. Second, we simulated poorly thermally equilibrated cluster anions by running simulations of neutral acetonitrile clusters and then simply attaching the excess electron, so that the clusters' ability to reorganize in the presence of excess electrons was highly limited. We find that the poorly equilibrated simulations provide the best match to the experimentally measured VEDEs for small cluster sizes and that isomer I corresponds to a surface-bound anion while isomer II is a solvated $(CH_3CN)_2^-$ anion. Moreover, when there is poor thermal equilibration at smaller cluster sizes, we see clear evidence for the formation of solvated acetonitrile monomer anions, and we believe that CH_3CN^-, rather than a vibronic sideband, explains the high-energy shoulder seen experimentally on the isomer I photoelectron peak.[8] The electron binding energies of all species increase in clusters with larger sizes and with better equilibration, and it appears that experimental cluster anions with sizes larger than those investigated here ($n > 12$) are more thermally equilibrated than smaller cluster anions. Overall, because of their generally poor thermal equilibration, the features seen in the photoelectron spectroscopy of small $(CH_3CN)_n^-$ cluster anions do not directly correspond to the excess electron species present in the bulk liquid.

■ COMPUTATIONAL METHODOLOGY

For our *ab initio* molecular dynamics simulations of $(CH_3CN)_n^-$ cluster anions, we chose to use dispersion-corrected density functional theory with the optimally tuned long-range-corrected (LRC) BNL functional[33,34] and the 6-31++G* basis set. Such a level of theory has previously been shown to accurately describe the energetics and dynamics of water cluster anions.[22] For all of our simulations, we used a 0.5 fs time step to simulate dynamics in the microcanonical (NVE)

ensemble at approximately room temperature starting from neutral configurations constructed with the Packmol software.[35] As discussed further below, we ran both room-temperature-equilibrated trajectories of anionic clusters and trajectories of neutral acetonitrile clusters to which an electron was suddenly added. For detailed analysis, we then quenched (i.e., geometry-optimized) uncorrelated anion configurations taken from these trajectories using the same optimized BNL functional with the larger 6-311++G** basis set (although we found that for the $n = 5$ cluster anion dynamics, the geometry optimization step did not change the observed distribution of electron binding motifs or VEDEs; see the Supporting Information for more details). Corrections due to dispersion were accounted for with the D3 empirical potential developed by Grimme,[36] as implemented in the quantum chemistry package Q-Chem 5.2.1.[37]

Before running any trajectories or extracting any configurations for geometry optimization, we first ensured that the range-separation parameter, ω, in the BNL functional was appropriately tuned for studying acetonitrile anion clusters. We began the functional optimization procedure by tuning the range-separation parameter to accurately describe both dipole and valence interactions between an excess electron and acetonitrile molecules in the gas phase. Two structures were considered for these initial gas-phase optimization calculations: a single linear acetonitrile dipole-bound anion and a bent antiparallel dimer anion. After individually optimizing the range-separation parameter for each anionic species, as described in more detail in the Supporting Information, we found that the optimally tuned parameter for the dimer anion was able to describe the ionization potential, dipole moment, and quadrupole moment of both the gas-phase dimer anion and the dipole-bound monomer species. Moreover, the optimally tuned functional also replicated the electronic properties of a bent monomer anion at the same level of theory.

We then optimized our long-range-corrected functional for cluster anion simulations by running an unbiased room-temperature $(CH_3CN)_5^-$ trajectory using the dimer anion's optimally tuned range-separation parameter ($\omega = 0.320$ bohr^{-1}). Following a 1.5 ps initial equilibration period, we extracted eight uncorrelated (at least 1000 fs apart) cluster anion structures and performed a geometry optimization on each of them. We then applied the functional-tuning scheme described above to each of the collected structures and used the optimized values to compute an average optimized range-separation parameter. The mean value ($\omega = 0.151$ bohr^{-1}) for the optimally tuned functional obtained this way was then used to run another DFT-based $(CH_3CN)_5^-$ BOMD simulation. We then extracted uncorrelated configurations from this latter run and reoptimized the range-separation parameter but found that the optimal average value of $\omega = 0.151$ bohr^{-1} did not change. We then tested the new optimally tuned functional on the original gas-phase species and found that we were able to replicate their ionization potential and dipole moment to an acceptable degree of accuracy. Thus, we settled on $\omega = 0.151$ bohr^{-1} as our optimally tuned range-separation parameter for all subsequent calculations and did not further adjust it for different cluster sizes or configurations.

With our chosen long-range-corrected BNL functional optimally tuned, we then studied the dynamics and energetics of $(CH_3CN)_n^-$ cluster anions of sizes $n = 5$, 7, and 10. The largest cluster size of 10 was chosen as a compromise between

offering the best comparison to experiment at larger sizes and computational expense. For the $n = 10$ cluster anion size, each *ab initio* MD step required roughly 300 CPU-s to complete when parallelized over 48 cores; since many picoseconds of dynamics was required for decent statistics and the step size was 0.0005 ps, $n = 10$ was the upper limit of computational feasibility. Including a 1.5 ps equilibration period, we were able to complete four 15 ps trajectories for $n = 5$ and five 13 ps trajectories for $n = 7$ cluster anions. For $n = 10$, we were only able to run two *ab initio* equilibrated trajectories of 4 and 9 ps duration.

The trajectories described above were all run at thermal equilibrium near room temperature, but experimentally, acetonitrile cluster anions are prepared by supersonic expansion,[8,9,38] so if they are at thermal equilibrium, they likely have a temperature much below 300 K. Moreover, the experimental clusters start with neutral acetonitrile vapor that is crossed with an electron beam before being mass-selected, so it is not at all clear that the experimental clusters ever achieve equilibrium in the presence of the excess electron. If the clusters do reach some type of equilibrium, their characteristic temperatures likely increase with cluster size because there is less evaporative cooling from larger clusters compared to smaller clusters. The problem is that there is no simple way to determine the experimental cluster temperature. This makes it challenging to directly compare simulations in thermal equilibrium at room temperature with the cluster anion experiments.

As an attempt to account for the unknown experimental cluster temperature, we analyzed simulated cluster anion configurations generated in two different ways, which are summarized in Figure 1. First, as indicated at the top of the figure, we extracted uncorrelated cluster anion configurations every 50 fs from the room-temperature equilibrium
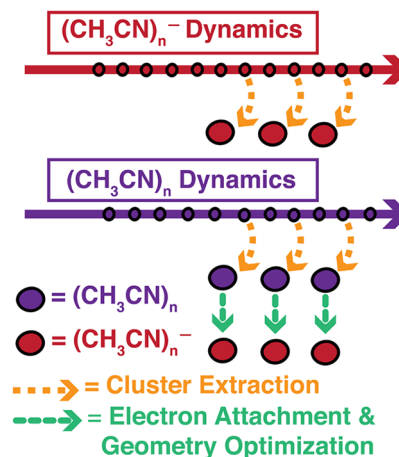
Figure 1. Schematic for generating *ab initio* configurations of both thermally equilibrated and poorly equilibrated $(CH_3CN)_n^-$ cluster anions. Top: thermally equilibrated (near room temperature) $(CH_3CN)_n^-$ cluster anion geometries were obtained by extracting uncorrelated configurations from an LRC-DFT-based *ab initio* trajectory of the anion. Bottom: cluster anions with poor thermal equilibration were constructed by extracting uncorrelated configurations from a classical neutral $(CH_3CN)_n$ trajectory, attaching an excess electron, and then performing a geometry-optimization calculation using the LRC DFT methodology described in the text. This dual approach is similar to what we used previously to describe water cluster anions in ref 22.

$(CH_3CN)_n^-$ trajectories described above. Second, as indicated in the lower part of the figure, using the classical molecular dynamics code LAMMPS,[39] we simulated poor thermal equilibration conditions/colder cluster temperatures by starting with *classical* MD trajectories of neutral acetonitrile clusters with sizes $n = 5$ and 10 using a flexible all-atom force field.[26,40] We then extracted uncorrelated neutral CH_3CN cluster configurations every 0.5 ps, added an excess electron, and then immediately quenched (i.e., geometry-optimized) these configurations using the methodology described above without running any *ab initio* dynamics. We note that we used a similar methodology in our previous study of water cluster anions and were able to successfully reproduce photoelectron spectroscopy experiments from different groups that used different cluster expansions conditions.[22]

Finally, to ensure that the use of classical trajectories on neutral acetonitrile cluster dynamics was a reasonable approach for the production of poorly equilibrated $(CH_3CN)_n^-$ cluster anions, we also produced poorly equilibrated cluster anions by first running DFT-based *ab initio* trajectories for neutral $n = 5$ clusters and then adding the excess electron and immediately performing a geometry optimization. We then compared the results from preparing the neutral clusters with classical mechanics versus preparing them using DFT and found no statistically significant difference between the distribution of different binding motifs observed or in the range of calculated VEDEs, as described in more detail in the Supporting Information. This gave us confidence that the use of classical mechanics for generating poorly equilibrated cluster anions at the larger $n = 10$ size produced meaningful configurations.

■ RESULTS AND DISCUSSION

Categorizing the Electron Binding Motifs in $(CH_3CN)_n^-$ Cluster Anions. After running trajectories and collecting both room-temperature-equilibrated and poorly equilibrated acetonitrile cluster anion configurations for clusters with sizes 5 and 10 (as well as equilibrated trajectories for size 7), we began our analysis by examining the dynamics of the individual acetonitrile molecules that make up each cluster anion. What we found is that the C−C−N bond angle, Θ_{CCN}, serves as a chemically meaningful order parameter that is capable of differentiating the binding motifs that we observe for the excess electron. The choice of Θ_{CCN} as an order parameter for understanding the excess electron behavior makes sense because this bond angle is strongly correlated to the electron affinity of the molecule: a single CH_3CN^- anion changes from dipole bound to valence bound as Θ_{CCN} changes from 180° to 130°.[6]

Figure 2 provides a limited sampling of how this bond angle typically changes as a function of time for all of the CH_3CN molecules in each of the cluster sizes tackled in the study; for the data displayed here, the dynamics were collected for $(CH_3CN)_n^-$ clusters at thermal equilibrium at roughly room temperature. What the data show is that there are three distinct distributions of Θ_{CCN}. For the $n = 5$ cluster anion, we see that at many times (for example, for the first ∼0.5 ps of the trajectory plotted) all five acetonitrile molecules have bond angles ≥155°, which we will refer to as "straight" molecules. What we will show below is that when all the molecules are straight, the electron is dipole bound to the surface of the cluster. Next, we see many configurations in both the $n = 5$ and $n = 10$ cluster anions where a single CH_3CN molecule had a bond angle between 125° and 155°, which we will refer to as
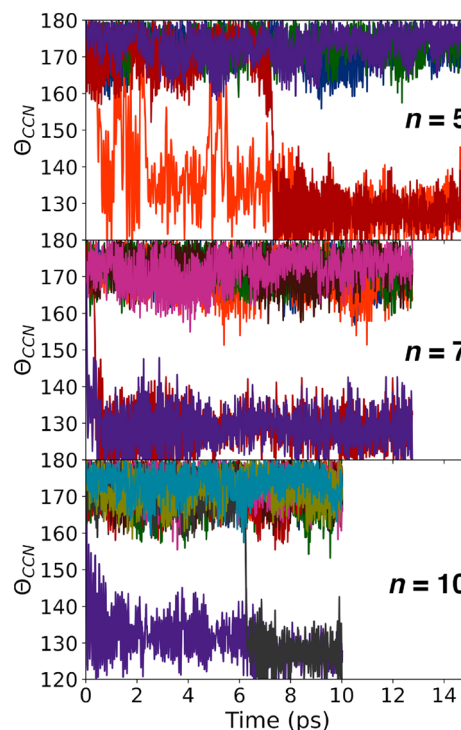
Figure 2. A limited sampling of the time evolution of the C−C−N bond angle, Θ_{CCN}, for all of the molecules comprising thermally equilibrated acetonitrile anion clusters of different sizes. From top to bottom are dynamical bond angle distributions for $(CH_3CN)_5^-$, $(CH_3CN)_7^-$, and $(CH_3CN)_{10}^-$ cluster anions. As discussed in the main text, three common bond-angle distributions were observed: $\Theta_{CCN} \geq 155.0°$ (straight) for all molecules, $\Theta_{CCN} < 155.0°$ (bent) for one molecule with the others straight, and $\Theta_{CCN} < 155.0°$ for two molecules with the rest straight.

"bent", while the other molecules in the cluster remained straight. We will show below that clusters with a single bent molecule have the excess electron associated almost entirely with that molecule, which we will refer to as a solvated CH_3CN^- monomer anion. Finally, we also see configurations (particularly for the $n = 7$ and $n = 10$ cluster anions) where there are two bent acetonitriles with the rest of the molecules in the cluster anion being straight; we will show below that the electron is associated with the two bent molecules, which are always adjacent in this case, corresponding to a solvated $(CH_3CN)_2^-$ dimer anion.

The way the excess electron behaves in clusters with different numbers of bent and straight CH_3CN molecules is summarized in Figure 3, which shows representative molecular geometries and excess electron spin densities for selected $n = 5$ cluster anion configurations. Panel A shows the case where all the molecules are straight. In this case, the excess electron largely extends away from the cluster into the vacuum and is not strongly associated with any particular molecule or molecules in the cluster. Panel B shows the case when there is a single bent molecule. Clearly, the excess electron's spin density is almost entirely associated with the bent molecule, essentially a valence-bound monomer anion stabilized by the dipoles of the neighboring straight molecules. Finally, panel C shows the case where there are two bent molecules. We see that the two bent molecules always appear adjacent and roughly aligned antiparallel, and the excess electron is
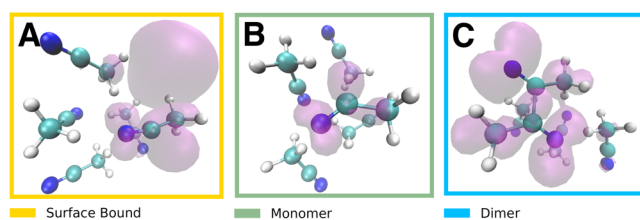
Figure 3. Representative snapshots showing the molecular geometry and excess electron spin density for the three distinct excess-electron binding motifs captured in our thermally equilibrated $n = 5$ BOMD simulations. From left to right we have (A) the surface-bound anion (no bent molecules), (B) the solvated monomer anion (one bent molecule), and (C) the solvated dimer anion (two bent molecules) binding motifs.

Figure 4. Relative abundance of different electron binding motifs of uncorrelated $n = 5$ (top) and $n = 10$ acetonitrile cluster anion configurations taken from poorly equilibrated trajectories (left) and room-temperature thermally equilibrated trajectories (right); the results for thermally equilibrated $n = 7$ clusters, which lie between those of the $n = 5$ and 10 clusters, are shown in the Supporting Information. The relative abundance of valence-bound monomer and dimer anions was seen to increase with cluster size, regardless of production methodology. Surface-bound anions are more predominant in poorly thermalized cluster anions, while thermal equilibration favored the formation of the valence-bound monomer and dimer molecular anion species.

distributed roughly uniformly over both molecules, forming a solvated molecular dimer anion.

To further understand the different types of excess electron binding motifs, we quantified the excess electron's spatial extent by investigating how the center of mass and radius of gyration of the excess electron's spin density compare to those of the entire cluster. We find (see the Supporting Information for more details) that solvated monomer and dimer anions (with one or two bent molecules, respectively) had relatively compact electron radii of gyration compared to the size of the cluster and that the center of the electron was on average located inside the cluster's radius of gyration. For surface-bound excess electrons (clusters with only straight molecules), we found that the electron's radius of gyration was comparable to or larger than that of the cluster and that the center of mass of the electron generally resided outside the cluster's radius of gyration. Thus, our assignment of these species as molecular and dipole-bound fits well with the position and spatial extent of the electron's spin density.

Figure 4 shows the relative abundance of the different types of electron binding motifs in clusters with different sizes and different production methodologies. The data in the leftmost panels were constructed from 78 and 32 poorly thermalized cluster anions for sizes $n = 5$ and $n = 10$, respectively. Those plots in the rightmost panels consist of 964 and 192 thermally equilibrated configurations directly taken from the cluster anion trajectories every 50 fs for sizes $n = 5$ and $n = 10$, respectively (Figure S5 shows similar data for thermally equilibrated $n = 7$ cluster anions). We find the surface-bound species predominates in clusters that were prepared with poor thermal equilibration, while the valence-bound monomer and dimer anion species appear to a greater extent in clusters that were thermally equilibrated. We also see that larger cluster sizes favor the dimer anion over the monomer anion and disfavor the surface-bound species. Finally, as discussed in the next section, we also examined the VEDEs of our cluster anions and find that each electron binding motif corresponds to a unique VEDE range, allowing us to make a tentative assignment of the peaks seen in the $(CH_3CN)_n^-$ cluster anion photoelectron spectroscopy experiments.

The relatively low abundance of the molecular anion species in the poorly equilibrated clusters is related to the need for these species to be stabilized by solvation. Upon examination of the different binding motifs (see the Supporting Information for details), we find that the bent molecules of the valence-bound molecular anions, and particularly the dimer anion, are stabilized by coordination of the H atoms on their methyl

groups with nitrogen atoms on nearby straight acetonitrile molecules through H···N interactions. We found that for the poorly equilibrated clusters an average of 2.9 solvent interactions are involved in the stabilization of the dimer anion, while for well-thermalized cluster anions the dimer anion was on an average solvated by four H···N interactions. Because a geometry optimization cannot sample as many different molecular configurations as a room-temperature molecular dynamics trajectory, it makes sense that the poorly thermalized cluster anions can not easily adopt geometries with the solvation environment needed to properly stabilize the dimer anion.

Binding Energies of the Different Electron Binding Motifs in $(CH_3CN)_n^-$ Cluster Anions. With the classification of the $(CH_3CN)_n^-$ excess electron binding motifs in hand, we turn next to understanding how these binding motifs relate to the VEDEs that are measured in photoelectron spectroscopy experiments. Figure 5 shows the distribution of binding energies (equal to the negative SOMO energy of the clusters since our long-range-corrected DFT functional was optimized for this purpose) for our properly and poorly thermalized $n = 5$ and $n = 10$ acetonitrile cluster anions. The y-axis illustrates the fraction of configurations that had a particular binding energy for each individual excess electron binding motif. The configurations used to generate these plots are the same ones used to construct Figure 4, and the data are color-coded to match the assigned electron binding motif. We see clearly that the surface-bound electron (yellow) has a very low VEDE. The monomer anion has only a slightly higher VEDE (green), while the dimer anion (blue) is much more strongly bound than either the monomer anion or surface-bound electron. For all three electron binding motifs, the VEDE increases slightly with increasing cluster size.
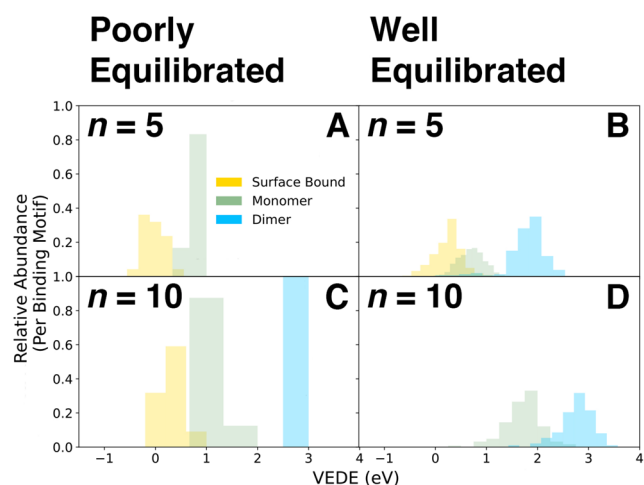
Figure 5. Vertical electron detachment energies of $(CH_3CN)_n^-$ anions from uncorrelated configurations extracted out of poorly thermalized trajectories (left) and thermally equilibrated trajectories (right) for clusters of size $n = 5$ (top) and $n = 10$ (bottom). Results for thermally equilibrated $n = 7$ clusters are shown in the Supporting Information. The configurations chosen are the same as those explored in Figure 4, and the data are color-coded to show the VEDEs for the different binding motifs (surface-bound = yellow; monomer anion = green; dimer anion = blue). The VEDEs increase in the order surface-bound, monomer anion, dimer anion, with the dimer anion electron being more than an electronvolt more stable than the other two species. The VEDEs of all three species increase with increasing cluster size.

With the VEDEs of our simulated cluster anions, we are now in a position to compare to the results of photoelectron spectroscopy experiments. In the experiments of Mitsui et al., the VEDEs of $(CH_3CN)_n^-$ cluster anions were measured down to a size of $n = 10$, providing a direct point of contact for our work.[8] Figure 6A compares the experimentally measured photoelectron spectrum for anion cluster size $n = 10$ (solid black curve) to those computed from our poorly thermalized $n = 10$ simulations (solid red curve). Excluding any negative VEDEs, the simulated spectrum for each binding motif was constructed from the data presented in Figure 5 by assuming a normal distribution and by using the maximum likelihood

estimation method to obtain the mean and standard deviation for its Gaussian function. These individual fits were added together to create the red curves presented in Figure 6. We see that the VEDE distributions of the poorly thermalized simulated clusters show remarkably good agreement with experiment, while the thermally equilibrated simulations, shown in Figure 6B, do not. This suggests that, indeed, the expansion conditions needed to create small $(CH_3CN)_n^-$ cluster anions do not provide an opportunity for the clusters to equilibrate in the presence of the excess electron.

On the basis of the generally good agreement between experiment and theory, we are now able to assign the peaks present in the experimental photoelectron spectroscopy of $(CH_3CN)_n^-$ cluster anions. First, the simulations clearly suggest that the weakly bound isomer I species is a surface-bound electron, similar to the species observed in previous studies of small water cluster anions.[22−24] We find no evidence that isomer I could be the cluster-phase counterpart to the bulk phase's cavity solvated electron: we never observe any type of interior (non-valence-bound) solvation of the electron in the cluster sizes we studied, and the fact that the experimental clusters are clearly poorly thermalized also helps rule out cavity electron binding motifs. Second, we can assign the low-intensity "shoulder" seen near 0.8 eV experimentally to detachment from the solvated CH_3CN^- monomer anion. We note that Mitsui et al. tentatively assigned this feature to a C−H stretching progression of the isomer I main peak. This assignment does not make sense to us, however, as it would require the main isomer I peak to have one quantum of excitation in the C−H stretch, which does not fit well with the fact that the clusters are likely poorly thermally equilibrated and have an effective temperature well below room temperature. Furthermore, it has been previously argued that monomer anions are the dominant species in solid-state β-acetonitrile, in which it is difficult for dimer anions to form because there is limited accessibility for neighboring molecules to align in the requisite antiparallel arrangement.[5] Thus, our reassignment of this feature to the monomer anion removes any assumptions about vibrational excitation in the clusters and is consistent with both this previous work and what we observe in the simulations. The fact that our simulations also reproduce the experimental observation that both the isomer I peak and
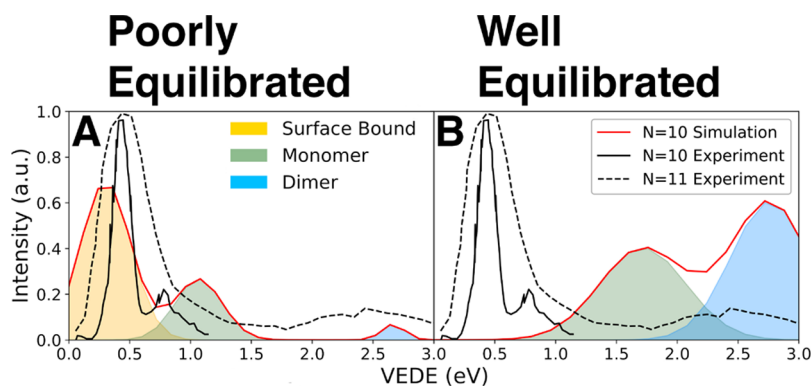
Figure 6. Experimental photoelectron spectra for $(CH_3CN)_{10}^-$ (solid black curve) and $(CH_3CN)_{11}^-$ (dashed black curve) cluster anions, taken from ref 8, are compared to the $(CH_3CN)_{10}^-$ VEDE distribution calculated from our simulations of size $n = 10$ based on Gaussian fits to the data as in Figure 5 to better represent the experimental energy resolution. In the left panel we compare the simulated spectrum for poorly equilibrated $(CH_3CN)_{10}^-$ clusters to the experimental measurements on the clusters of size $n = 10$ and $n = 11$. The right panel compares the same experimental spectra to our thermally equilibrated $(CH_3CN)_{10}^-$ cluster anion calculated VEDE distribution. The individual contributions of the surface-bound, monomer, and dimer anion to the simulated data are emphasized by the color-shaded regions.

the associated shoulder shift to higher binding energies with increasing cluster size also supports our assignment of the two features to the surface-bound electron and monomer anion.

Finally, in agreement with the general consensus in the literature,[5,8,9,38] we believe that the isomer II peak, which becomes prominent at higher binding energies in the experimental photoelectron spectra at cluster sizes $n \geq 12$, is due to the $(CH_3CN)_2^-$ dimer anion. We note that experimental studies on low-temperature solid-state α-acetonitrile crystals have also argued that the absorption band observed in the UV/blue portion of the spectrum for the bulk solvated electron can be explained as arising from the dimer anion.[5]

Figure 6 also compares the high-energy range of our simulated spectrum for $n = 10$ with the experimental photoelectron spectrum for $n = 11$ (dashed black curve).[8] We make this comparison because $n = 11$ is the smallest cluster size for which the isomer II peak is somewhat visible, and we see that the position and relative intensity of this peak agree reasonably well with the predictions for the dimer anion from our poorly thermally equilibrated simulations. What this comparison suggests is that the experimental clusters of this size are even more poorly equilibrated (or at a colder average temperature) then the way we simulated them from room-temperature neutral cluster configurations: we see a slightly larger population of dimer anions in our simulations because the geometry-optimization procedure we use is better able to provide the requisite H···N interactions needed to stabilize this species than the colder cluster anions created experimentally. We note that the experiments also show that the isomer II peak becomes predominant by size $n \geq 13$. We believe that this occurs for two reasons. First, the larger clusters have more straight molecules that can provide favorable solvation interactions to help stabilize the formation of a dimer anion. Second, the larger clusters in the experiments are also likely more thermally equilibrated than the smaller clusters, so that the relative distribution of electron binding motifs for clusters with $n \geq 13$ starts to resemble that of the thermally equilibrated trajectories in our simulations more than the poorly equilibrated trajectories, again favoring the dimer anion.

■ CONCLUSIONS

In summary, we have carefully tuned the range-separation parameter of the BNL functional to capture the chemistry of acetonitrile cluster anions to a reasonable level of quantum chemical accuracy. With the optimally tuned functional, we studied the energetics and dynamics of $(CH_3CN)_n^-$ cluster anions with sizes $n = 5$, 7, and 10. The simulations revealed that the electron has three chemically distinct binding motifs. For the weakest binding motif, the surface-bound anion, the electron is attached to the cluster largely through dipole interactions. The other two binding motifs have the electron valence bound as part of solvated molecular anions consisting of either one or two bent acetonitrile molecules stabilized through N···H interactions with the neighboring solvent molecules. The molecular dimer anion adopts an antiparallel structure and has a much higher electron binding energy than the monomer anion. In agreement with experiment, we observed a systematic shift toward higher energies in the distribution of binding energies with increasing cluster size for all three binding motifs.

We also compared the electron-binding behavior of acetonitrile cluster anions with sizes $n = 5$ and $n = 10$ when the clusters were either thermally equilibrated at room temperature or poorly equilibrated. We found that the formation of valence-bound monomer and dimer anions was favored with thermal equilibration, while clusters that were not properly thermalized preferred to have the excess electron be surface-bound, similar to what has been seen for small water cluster anions. A comparison of our simulated binding energies for $n = 10$ cluster anions to the experimental photoelectron spectra suggests that the experiments likely are studying poorly thermalized clusters and that the two primary isomers observed are the surface-bound electron and the molecular dimer anion. Our simulations also indicate that the monomer anion might be stably produced, particularly in poorly thermally equilibrated clusters, and we assign the shoulder seen on the lower-binding-energy peak in the experimental spectrum to this species.

Overall, our results suggest that the two isomers observed in $(CH_3CN)_n^-$ cluster anions do not correspond to the two types of excess electron species in bulk liquid acetonitrile. If we attempt to extrapolate the behavior of our thermally equilibrated cluster anion simulations to solution, we would argue that the monomer anion likely will not be stable relative to the dimer anion because in bulk solution there will always be a place where two acetonitrile molecules can be antiparallel and well solvated if binding an excess electron. Thus, the two excess electron species present in the room-temperature liquid must be the cavity solvated electron and the solvated dimer anion. The precursor to the cavity solvated electron species must appear only at much larger cluster sizes than we have investigated here; the clusters must be large enough that the solvation energy provided by the dipoles of enough straight acetonitrile molecules pointing toward the cavity overcomes the stabilization and solvation of the valence-bound dimer anion. This is not something that happens easily because even in bulk solution at room temperature, equilibrium still favors the formation of the valence dimer anion by a factor of 4.[1] It would be interesting for future work to study the behavior of larger, better thermally equilibrated $(CH_3CN)_n^-$ cluster anions to see if the precursor state to the bulk cavity solvated electron can be directly observed or if the fact that gas-phase cluster anions are generally poorly equilibrated means that it is not possible to extrapolate from clusters to the bulk when excess electrons are involved.

■ ASSOCIATED CONTENT

ⓢ Supporting Information

The Supporting Information is available free of charge at https://pubs.acs.org/doi/10.1021/acs.jpca.1c05855.

> Long-range-corrected functional optimization; poorly equilibrated $(CH_3CN)_n$ cluster dynamics: classical vs LRC DFT; the role of geometry optimization in $(CH_3CN)_n^-$ electron binding motif electron location; and degree of localization in different binding motifs; LRC-DFT $(CH_3CN)_n^-$ BOMD dynamics; solvation stabilizes the acetonitrile dimer anion; Figures S1−S6 and Tables S1−S3 (PDF)

■ AUTHOR INFORMATION

Corresponding Author

Benjamin J. Schwartz − *Department of Chemistry and Biochemistry, University of California, Los Angeles, Los*

Angeles, California 90095-1569, United States; orcid.org/0000-0003-3257-9152; Email: schwartz@chem.ucla.edu

Author

Wilberth A. Narvaez − *Department of Chemistry and Biochemistry, University of California, Los Angeles, Los Angeles, California 90095-1569, United States*

Notes

The authors declare no competing financial interest.

REFERENCES

(1) Doan, S. C.; Schwartz, B. J. Nature of Excess Electrons in Polar Fluids: Anion-Solvated Electron Equilibrium and Polarized Hole-Burning in Liquid Acetonitrile. *J. Phys. Chem. Lett.* **2013**, *4*, 1471−1476.

(2) Shkrob, I. A.; Sauer, M. C. Electron Localization in Liquid Acetonitrile. *J. Phys. Chem. A* **2002**, *106*, 9120−9131.

(3) Xia, C.; Peon, J.; Kohler, B. Femtosecond Electron Ejection in Liquid Acetonitrile: Evidence for Cavity Electrons and Solvent Anions. *J. Chem. Phys.* **2002**, *117*, 8855−8866.

(4) Doan, S. C.; Schwartz, B. J. Ultrafast Studies of Excess Electrons in Liquid Acetonitrile: Revisiting the Solvated Electron/Solvent Dimer Anion Equilibrium. *J. Phys. Chem. B* **2013**, *117*, 4216−4221.

(5) Shkrob, I. A.; Takeda, K.; Williams, F. Electron Localization in Solid Acetonitrile. *J. Phys. Chem. A* **2002**, *106*, 9132−9144.

(6) Timerghazin, Q. K.; Peslherbe, G. H. Electronic Structure of the Acetonitrile and Acetonitrile Dimer Anions: A Topological Investigation. *J. Phys. Chem. B* **2008**, *112*, 520−528.

(7) Azar, J.; Kurlancheek, W.; Head-Gordon, M. Characterization of Electronically Excited States in Anionic Acetonitrile Clusters. *Phys. Chem. Chem. Phys.* **2011**, *13*, 9147−9154.

(8) Mitsui, M.; Ando, N.; Kokubo, S.; Nakajima, A.; Kaya, K. Coexistence of Solvated Electrons and Solvent Valence Anions in Negatively Charged Acetonitrile Clusters, $(CH_3CN)_n^-$ (n = 10−100). *Phys. Rev. Lett.* **2003**, *91*, 153002.

(9) Young, R. M.; Griffin, G. B.; Kammrath, A.; Ehrler, O. T.; Neumark, D. M. Time-Resolved Dynamics in Acetonitrile Cluster Anions $(CH_3CN)_n^-$. *Chem. Phys. Lett.* **2010**, *485*, 59−63.

(10) Coe, J. V.; Earhart, A. D.; Cohen, M. H.; Hoffman, G. J.; Sarkas, H. W.; Bowen, K. H. Using Cluster Studies to Approach the Electronic Structure of Bulk Water: Reassessing the Vacuum Level, Conduction Band Edge, and Band Gap of Water. *J. Chem. Phys.* **1997**, *107*, 6023−6031.

(11) Bragg, A. E.; Verlet, J. R. R.; Kammrath, A.; Cheshnovsky, D.; Neumark, D. N. Hydrated Electron Dynamics: From Clusters to Bulk. *Science* **2004**, *306*, 669−671.

(12) Verlet, J. R. R.; Bragg, A. E.; Kammrath, A.; Cheshnovsky, D.; Neumark, D. N. Observation of Large Water-Cluster Anions with Surface-Bound Excess Electrons. *Science* **2005**, *307*, 93−96.

(13) Neumark, D. M. Spectroscopy and Dynamics of Excess Electrons in Clusters. *Mol. Phys.* **2008**, *106*, 2183−2197.

(14) Ma, L.; Majer, K.; Chirot, F.; von Issendorff, B. Low Temperature Photoelectron Spectra of Water Cluster Anions. *J. Chem. Phys.* **2009**, *131*, 144303.

(15) Young, R. M.; Yandell, M. A.; King, S. B.; Neumark, D. M. Thermal Effects on Energetics and Dynamics in Water Cluster Anions $(H_2O)_n^-$. *J. Chem. Phys.* **2012**, *136*, 094304.

(16) Turi, L. Hydrated Electrons in Water Clusters: Inside or Outside, Cavity or Noncavity? *J. Chem. Theory Comput.* **2015**, *11*, 1745−1755.

(17) Madarász, Á.; Rossky, P. J.; Turi, L. Interior- and Surface-Bound Excess Electron States in Large Water Cluster Anions. *J. Chem. Phys.* **2009**, *130*, 124319.

(18) Jou, F.-Y.; Freeman, G. R. Temperature and Isotope Effects on the Shape of the Optical Absorption Spectrum of Solvated Electrons in Water. *J. Phys. Chem.* **1979**, *83*, 2383−2387.

(19) Turi, L.; Borgis, D. Analytical Investigations of an Electron-Water Molecule Pseudopotential. II. Development of a New Pair Potential and Molecular Dynamics Simulations. *J. Chem. Phys.* **2002**, *117*, 6186−6195.

(20) Jacobson, L. D.; Herbert, J. M. A One-Electron Model for the Aqueous Electron that Includes Many-Body Electron-Water Polarization: Bulk Equilibrium Structure, Vertical Electron Binding Energy, and Optical Absorption Spectrum. *J. Chem. Phys.* **2010**, *133*, 154506.

(21) Larsen, R. E.; Glover, W. J.; Schwartz, B. J. Does the Hydrated Electron Occupy a Cavity? *Science* **2010**, *329*, 65−69.

(22) Zho, C.-C.; Vlček, V.; Neuhauser, D.; Schwartz, B. J. Thermal Equilibration Controls H-Bonding and the Vertical Detachment Energy of Water Cluster Anions. *J. Phys. Chem. Lett.* **2018**, *9*, 5173−5178.

(23) Madarász, Á.; Rossky, P. J.; Turi, L. Response of Observables for Cold Anionic Water Clusters to Cluster Thermal History. *J. Phys. Chem. A* **2010**, *114*, 2331−2337.

(24) Jacobson, L. D.; Herbert, J. M. Theoretical Characterization of Four Distinct Isomer Types in Hydrated-Electron Clusters, and Proposed Assignments for Photoelectron Spectra of Water Cluster Anions. *J. Am. Chem. Soc.* **2011**, *133*, 19889−19899.

(25) Takayanagi, T. Theoretical Simulations of Dynamics of Excess Electron Attachment to Acetonitrile Clusters. *Chem. Phys.* **2004**, *302*, 85−93.

(26) Grabuleda, X.; Jaime, C.; Kollman, P. A. Molecular Dynamics Simulation Studies of Liquid Acetonitrile: New Six-Site Model. *J. Comput. Chem.* **2000**, *21*, 901−908.

(27) Abdoul-Carime, H.; Desfrançois, C. Electrons Weakly Bound to Molecules by Dipolar, Quadrupolar or Polarization Forces. *Eur. Phys. J. D* **1998**, *2*, 149−156.

(28) Takayanagi, T. Ab Initio Study of Small Acetonitrile Cluster Anions. *J. Chem. Phys.* **2005**, *122*, 244307.

(29) Takayanagi, T.; Hoshino, T.; Takahashi, K. Electronic Structure Calculations of Acetonitrile Cluster Anions: Stabilization Mechanism of Molecular Radical Anions by Solvation. *Chem. Phys.* **2006**, *324*, 679−688.

(30) Takayanagi, T. Dynamical Calculations of Charge-Transfer-to-Solvent Excited States of Small I^- $(CH_3CN)_n$ Clusters. *J. Phys. Chem. A* **2006**, *110*, 7011−7018.

(31) Nigam, S.; Majumder, C. Growth Pattern and Electronic Properties of Acetonitrile Clusters: A Density Functional Study. *J. Chem. Phys.* **2008**, *128*, 214307.

(32) Remya, K.; Suresh, C. H. Cooperativity and Cluster Growth Patterns in Acetonitrile: A DFT Study. *J. Comput. Chem.* **2014**, *35*, 910−922.

(33) Livshits, E.; Baer, R. A Well-Tempered Density Functional Theory of Electrons in Molecules. *Phys. Chem. Chem. Phys.* **2007**, *9*, 2932−2941.

(34) Baer, R.; Neuhauser, D. Density Functional Theory with Correct Long-Range Asymptotic Behavior. *Phys. Rev. Lett.* **2005**, *94*, 043002.

(35) Martínez, L.; Andrade, R.; Birgin, E. G.; Martínez, J. M. PACKMOL: A Package for Building Initial Configurations for Molecular Dynamics Simulations. *J. Comput. Chem.* **2009**, *30*, 2157−2164.

(36) Grimme, S. Semiempirical GGA-Type Density Functional Constructed with a Long-Range Dispersion Correction. *J. Comput. Chem.* **2006**, *27*, 1787−1799.

(37) Shao, Y.; Gan, Z.; Epifanovsky, E.; Gilbert, A. T.; Wormit, M.; Kussmann, J.; Lange, A. W.; Behn, A.; Deng, J.; Feng, X.; et al.

Advances in Molecular Quantum Chemistry Contained in the Q-Chem 4 Program Package. *Mol. Phys.* **2015**, *113*, 184−215.

(38) Young, R. M.; Neumark, D. M. Dynamics of Solvated Electrons in Clusters. *Chem. Rev.* **2012**, *112*, 5553−5577.

(39) Plimpton, S. Fast Parallel Algorithms for Short-Range Molecular Dynamics. *J. Comput. Phys.* **1995**, *117*, 1−19.

(40) Howard, A. E.; Cieplak, P.; Kollman, P. A. A Molecular Mechanical Model that Reproduces the Relative Energies for Chair and Twist-Boat Conformations of 1,3-Dioxanes. *J. Comput. Chem.* **1995**, *16*, 243−261.